

Numerical simulation of the abrupt occurrence of strong current in the southeastern Japan Sea

Naoki HIROSE (Research Institute for Applied Mechanics, Kyushu University, 6-1 Kasuga-kouen, Kasuga 816-8580, Japan)

Yutaka KUMAKI (Kyoto Prefectural Agriculture, Forestry and Fisheries Technology Center, 1029-3 Odashukuno, Miyazu 626-0052, Japan)

Atsushi KANEDA (Faculty of Marine Bioscience, Fukui Prefectural University, 1-1 Gakuen, Obama 917-0003, Japan)

Kouta AYUKAWA (Fukui Prefectural Fisheries Experimental Station, 23-1 Urasoko, Tsuruga 914-0843, Japan)

Noriyuki OKEI (Ishikawa Prefecture Fisheries Research Center, 3-7 Ushitsu-shinko, Noto 927-0435, Japan)

Satoshi IKEDA (Niigata Prefectural Fisheries and Marine Research Institute, 3-13098-8 Ikarashi, Nishi, Niigata 950-2171, Japan)

Yosuke IGETA (Japan Sea National Fisheries Research Institute, Fisheries Research and Education Agency, 1-5939-22 Suido-cho, Chuo, Niigata 951-8121, Japan)

Tatsuro WATANABE (Japan Sea National Fisheries Research Institute, Fisheries Research and Education Agency, 1-5939-22 Suido-cho, Chuo, Niigata 951-8121, Japan)

Highlights

- Rapid changes of coastal current damaging set-net fisheries accurately modeled in the Japan Sea.
- High-resolution prediction of the stormy current successful in Wakasa, Toyama, and Ryotsu Bays.
- Most of the kyucho occurrences in this area can be attributed to severe meteorological disturbances.
- Presence of seasonal stratification is necessary for the intensification of surface current.
- Downstream eddy separated from Tango Peninsula often grows into bay-scale anticyclonic eddy.

Abstract

Coastal set-net fisheries have been frequently damaged by the occurrence of sudden current (known as kyucho) in the Japan Sea. In this study, a high-resolution coastal ocean model is developed to provide a means to predict this stormy current. The 1.5km-mesh model nested in a regional ocean data assimilation system is driven by mesoscale atmospheric conditions at 1-hour intervals. The modeled results show rapid changes of the coastal current along the San-in Coast, on the eastern side of the Tango Peninsula, and around the Noto Peninsula and Sado Island, mostly associated with strong wind events. These modeled coastal water responses are consistent with in-situ velocity measurements. The simulation also shows that the vortex separated from the Tango Peninsula frequently grows to a bay-scale anticyclonic eddy in Wakasa Bay. Evidently, the coastal branch of the Tsushima Warm Current becomes unstable due to a strong meteorological disturbance resulting in the generation of this harmful eddy.

Keywords

stormy current, kyucho, set-net fishery, ocean general circulation model, coastal current, Japan Sea

1. Introduction

Numerical simulation and prediction of abrupt change in the nearshore current were successfully established for the eastern side of the Noto Peninsula by Asa et al. (2007) and Nakada et al. (2014). The strong and rapid coastal current, sometimes associated with shocking temperature change, has been empirically called “kyucho” in Japan. Since the major cause of kyucho in the southern Japan Sea has already been identified to meteorological disturbances, the numerical forecast was demonstrated to be a useful tool to help preparation for this stormy current (Nakada et al., 2014). The modeling ability to predict the kyucho occurrences, together with the efforts of local governments and fishery operators, actually contributes to reduce damages to set-net fisheries in Toyama Bay (Okei et al., 2012).

In this study, we extend and improve the numerical model of Nakada et al. (2014). The set-nets have been occasionally destroyed by rapid kyucho currents in Toyama Bay as well as along the San-in Coast, in Wakasa Bay and Ryotsu Bay, and in other coastal waters (e.g., Maruyama, 2009a). Each set-net structure is quite large (on the order of 1 km), and thus the total financial damage to the hundreds of structures can exceed one billion Japanese Yen after even one event.

Among these waters, in-situ measurement efforts of strong currents have been well documented for Wakasa Bay. For example, Kumaki (2012) reports in detail the characteristics of the kyuchos around the Tango Peninsula along with a discussion of the physical processes. He concludes that most of the measured strong currents around the Tango Peninsula were caused by wave propagations excited by strong winds such as those from typhoons. In terms of numerical modeling, Umatani and Yamagata (1987), Igeta et al. (2007), and Kumaki et al. (2012) clarify the physical processes of sudden current based on an idealized representations of the conditions in this region.

Kumaki (2012) also mentions that several cases of kyucho (statistically less than 10%) remain unexplained solely by the wind forcing. One possibility is a clockwise eddy formed in Wakasa Bay. The bay-scale anticyclonic circulation was initially reported by Uda (1931). Later, Wada and Yamada (1997) categorized the flow patterns based on acoustic Doppler current profiler (ADCP) measurement in Wakasa Bay. The former studies also suggested the relationship with the coastal branch of the Tsushima Warm Current (TWC) from San-in Coast.

These studies imply that we need to consider realistic conditions such as the TWC system including mesoscale eddies, complex horizontal and vertical mixing processes, or high-resolution wind forcing in time and space, to simulate various types of the stormy

currents. For instance, none of the previous modeling studies considered the effect of incoming coastal currents on the generation of sudden current in Wakasa Bay.

The threatening situation of kyucho at San-in Coast, Sado Island, and other set-net fishery areas may be more or less similar to Wakasa Bay (e.g., Maruyama, 2009a, b). Therefore, this study aims to provide a more realistic numerical simulation of the rapid change in nearshore currents along the complex coastline of the total extension over 2500km (Fig. 1). For this purpose, a high-resolution model may be required as suggested by the previous numerical studies (Igeta et al., 2007; Kumaki et al., 2012; Nakada et al., 2014). In this paper, the effect of grid spacing will be examined by comparison with the large-scale model already provided by Hirose et al. (2013). Then we will examine the important factors and processes affecting our ability to predict kyuchos.

2. Model configuration

In this study, we develop a new coastal ocean model. Since the target area is limited to *coastal* waters (Fig. 1), we name it DR_C. The open boundary condition is given by a regional, eddy-resolving, data assimilation model (Hirose et al., 2013) in one-way connection at the north and western faces. The parent model covers the two *marginal* seas of the Japan and East China Seas and is thus abbreviated as DR_M. The diagonal interface between the two models is configured from 36°N, 132°E to 40°N, 137°E considering the parallel computing efficiency with the Message Passing Interface (MPI) program of the RIAM Ocean Model (Lee et al., 2003). The provided variables from DR_M to DR_C are the sea surface height, temperature, salinity, and horizontal velocity components.

The RIAM Ocean Model is a z-coordinate primitive OGCM with Arakawa's B-grid spacing on the spherical coordinate developed originally by Lee (1996) and Lee et al. (2003). The generalized Arakawa scheme is used for the advection term in the horizontal momentum equations. We follow the formulation suggested by Ishizaki and Motoi (1999) including the slant advection effect. The governing equations are separated into barotropic and baroclinic modes and thus allow longer time steps for internal dynamics.

The earlier version of the high-resolution coastal model was developed by Nakada et al. (2014) for a small region around the Noto Peninsula or Ishikawa Prefecture. This result will be distinguished by DR_I. The major differences of the three models (DR_M, DR_I, and DR_C) are given in Table 1.

The bottom topography of DR_C is given by a simple average of JTOPO30v2 (Marine

Information Research Center) and J-EGG500 (JODC-Expert Grid data for Geography-500m) as shown in Fig. 1b. The J-EGG500 covers the coastal area only and the offshore topography of this model is equivalent to JTOPO30v2. In addition, coastal grids are often corrected manually to maintain the realistic coastlines in this finite-resolution model to generate small channels (such as Douzen Islands of Oki) or to create small islands and banks (such as Kanmuri Island in western Wakasa Bay or Gentatsu Bank near the Echizen-Kaga Coast).

The numerical integration starts at January 1, 2010 with the initial condition interpolated from the parent model of DR_M. The first half year is basically wasted as the spin-up period and the following three months of July, August, and September are the main analysis period of this study since many damages have been reported in this season.

The surface meteorological condition is given by the operational meso-scale model (MSM) from the Japan Meteorological Agency (JMA). The spatial and temporal resolutions of MSM are quite high, being 5 km and 1 hour, respectively. Its surface meteorological variables (air temperature T_a , specific humidity q_a , cloud amount C , precipitation P , and wind vector \vec{U}_a) are linearly interpolated in time and space into the resolutions of the DR_C model.

The horizontal grid spacings of 1' and 0.8' for zonal and meridional directions in the DR_C are the same as in the DR_I. The vertical resolution of 2m in the DR_C is higher than that of 8m in the DR_I for the top layer. Similarly, the time step of the barotropic mode (2 seconds) stays the same as the DR_I model, but the baroclinic interval (20 seconds) is half of the earlier version to better resolve the high-frequency changes and strong advection near the surface. The modeled result is basically stored at 1-hour intervals.

The surface heat flux components are estimated by using empirical formulas similar to Hirose et al. (1996). This means that the cloud amount of MSM is used to estimate both short and long wave radiation at 1-hour intervals. An improvement is made on the surface current effect relative to the wind vector; the turbulent fluxes of wind stress, evaporation, and sensible heat are given by

$$\vec{\tau} = \rho_a c_D |\vec{U}_a - \vec{U}_s| (\vec{U}_a - \vec{U}_s) \quad (1)$$

$$E = \rho_a c_E |\vec{U}_a - \vec{U}_s| (q_a - q_s) \quad (2)$$

$$Q_h = \rho_a c_a c_H |\vec{U}_a - \vec{U}_s| (T_a - T_s) \quad (3)$$

respectively. The non-dimensional bulk coefficients c_D , c_E , and c_H are determined by Kondo (1975). The relative difference of atmosphere-ocean velocity $\vec{U}_a - \vec{U}_s$ is used explicitly here instead of the surface wind vector \vec{U}_a alone. The sea surface current and temperature (\vec{U}_s and T_s) are taken from the DR_C model directly at every baroclinic time step and the saturated specific humidity q_s is estimated by Gill (1982). The river discharges are also accounted for by the coastal precipitation as Hirose (2011).

The horizontal and vertical advection of temperature and salinity is modeled by the Modified-Split Quadratic Upstream Interpolation for Convective Kinematics (Webb et al., 1998) and Monotonic Second-Order Upwind (Sweby, 1984) schemes, respectively. The lateral eddy diffusion is characterized by a combination of isopycnal, thickness, and Cartesian operators (Gent and McWilliams, 1990). Their coefficients are identical at $2.5 \text{ m}^2/\text{s}$ in this DR_C model.

The vertical mixing near the surface is modeled by Noh and Kim (1999) with a reduced dependence on stratification ($\alpha = 50$) in their equation (17). The background coefficients for vertical viscosity and diffusion are set to be 1.0 and $0.2 \text{ cm}^2/\text{s}$.

The horizontal eddy viscosity is parameterized by Smagorinsky (1963) with a non-dimensional coefficient of 0.18 . The bottom friction is given by a quadratic form with a non-dimensional coefficient of 2.7×10^{-3} . In addition, the biharmonic form of eddy viscosity parameterization is applied only near the open boundary to damp the mismatches between the parent and child models. The biharmonic coefficient is reduced quadratically from with maximum value of $6 \times 10^8 \text{ m}^4/\text{s}$ at the boundary to zero at 15 km apart. On the other hand, the temperature and salinity field of DR_C is relaxed everywhere to the parent model of DR_M with a time scale of 15 days to maintain the realistic background conditions of TWC and mesoscale eddies. Instead, data assimilation of satellite data, such as remotely-sensed SST, is not applied to this model.

3. Results

3.1 Typical kyucho sequence

The typical surface water response to the passage of a typhoon is explained by using the DR_C model result. Typhoon 1004 (DIANMU) traveled from the west to the east of the study area on August 11 and 12, 2010 in the coordinate universal time (UTC). Its central positions can be traced at 6-hour intervals in Fig. 2. This typhoon was not very strong, as indicated by the central pressure around 994 hPa in this period. However,

strong surface current was excited by this dissipating typhoon as shown in Figs. 2 and 3. The water speed exceeded 1.0 m/s throughout most of the calculation area. The offshore current started to turn right, or in the clockwise direction, immediately after the typhoon passed (Fig. 2), which is basically recognized as the inertial oscillation (Asa et al., 2007; Igeta et al., 2007).

Fig. 3a also confirms that the absolute velocity was weaker than 1.0 m/s near the coastlines. Strong friction at the bottom and side boundaries seems to have retarded the flow of the coastal water.

However, the weaker speed does not mean weaker damages. In Fig. 3b, the maximum water speed is divided by the normal condition as defined by the three-month average from July to September, 2010. The offshore magnitude of velocity was about 3 or 4 times larger than the normal condition. This factor is a direct effect of the response to DIANMU.

Interestingly, the normalized speed was often stronger than 6 or 8 for the coastal water as shown by Fig. 3c-f. This is especially apparent in the small bays. These large anomalies can be hazardous to the set-net fisheries. An abrupt strong current (kyucho) can also be found on the east side of the Noto Peninsula in Fig. 2d. Numerical results will be analyzed for individual regions in the following sections. However, we can confirm here that the surface water response to a typhoon is not homogeneous and can even be amplified near the meandering coastline.

3.2 Toyama Bay

Here we examine two cases of the strong current occurrences that were successfully simulated along the eastern coast of the Noto Peninsula (or the northwestern part of Toyama Bay) in summer 2010. Both were excited by meteorological disturbances over the Japan Sea. The meteorological forcing for the first case was relatively weaker and was associated with a low pressure system that traveled along the Baiu front on July 11, 2010. The second one was excited by traveling DIANMU one month later as shown in Fig. 2.

The modeled response is compared with the former models of DR_M (Hirose et al., 2013) and DR_I (Nakada et al., 2014) in Fig. 4. All of the model results simulate well the kyucho arrival at 6-8Z of 7/12. The packet of kinetic energy propagated from the northern side of the Noto Peninsula with the inertial time scale (Asa et al., 2007). Actually, the strong surface current was already excited at 15-17Z of the previous day, north of the Noto Peninsula, as a direct response to southerly and southwesterly winds. In the bay area, local maxima were found later than a half day (cf., inertial period \sim 20 hour at

36.87°N).

However, the detailed structure of the three model results is slightly different as shown in Fig. 4. The lower resolution of the DR_M model produced only monotonic variation of the strong current. The central velocity is amplified in the DR_I but the horizontal scale of the stormy current is similar to the DR_M, probably due to the large viscosity coefficient that was chosen to ensure the numerical stability. The new model shows considerably smaller-scale features. The strong kinetic energy hits the coastline at around 37.3°N, 137.25°E, and bifurcates westward and northward in Fig. 4c. North of the Noto Peninsula, the northeastward current of the DR_C is stronger than that of the DR_I, probably for the same reason. The non-dimensional Smagorinsky coefficient (0.18) adopted here is much smaller than the uniform coefficient ($23 \times 10^8 \text{ m}^4/\text{s}$) of biharmonic viscosity in Nakada et al. (2014). By assuming a strong shear of 0.5 m/s over one grid interval ($\sim 1.5 \text{ km}$), the former coefficient is nearly equivalent to $100 \text{ m}^2/\text{s}$. The latter can be converted to a harmonic coefficient of $\sim 8200 \text{ m}^2/\text{s}$ at the same grid scale by using the relationship of Griffies and Hallberg (2000).

Detailed comparisons with in-situ measurements of surface currents near the coastline are provided in Fig. 5. The seawater velocity was measured at 10m depth near the locations of set-net structures by electromagnetic current meters (Okei et al., 2012). The alongshore velocity component is shown here since the cross-shore component is much weaker near the coastline. The local time-series from each model were estimated by bilinear interpolation using the surrounding 4-point grid values of the simulated velocity components. The water speed over land was assumed to be zero.

At first glance, near-inertial motions are clearly dominant, as shown in these time-series. These near-inertial motions possibly lasted for a week or longer as shown by Asa et al. (2007).

We can also confirm a fair level of consistency between the in-situ measurement and the model results in these diagrams. In other words, the statistical differences are insignificant between the three model simulations in comparisons with the measurement data. If we look carefully, the new model may be good at simulating the second or third maxima/minima in N2. On the other hand, the simulated amplitude is quite weak with the DR_M model because the short distance from the coastline ($\sim 2 \text{ km}$) cannot be resolved by the coarse resolution. The coastal waves propagating from N1 to N2 might be better simulated with the higher resolution models as these features are also shown in the DR_I model (Nakada et al., 2014).

An additional experiment was performed to understand the effect of stratification. The surface wind conditions from July to September were applied to this experiment for

three months beginning in January 2010. The surface layers are well mixed vertically in this winter condition. The result shows that the strong current hardly appears near the coastline (not shown). The offshore inertial motion directly excited by the surface wind change was weak in this experiment. The surface momentum quickly spread to the whole mixed layer over 100 m depth in winter and thus the surface response of the inertial motion was relatively weaker than that in summer. The vertically-homogeneous current hardly intruded into the inshore or coastal zones due to strong frictions at the bottom and/or side boundaries of the model. We recognize here that the presence of seasonal stratification is a necessary condition for the intensification of the surface current.

3.3 Ryotsu Bay

The present DR_C model also simulated realistic kyucho occurrences in Ryotsu Bay, on the eastern side of Sado Island probably for the first time. According to this simulation, a packet of strong kinetic energy generated by DIANMU propagated from north to east in August 12 (Fig. 6a-c). This dangerous motion turned to the right due to the inertial effect and hit the coastline at around 15Z the same day. The distance from the northern tip of Sado Island (Hazikizaki) to the hitting point (>20 km) is consistent with the diameter of the inertial circle expected from the core speed (~1 m/s with the inertial period ~ 19.5 hour at 38°N). This diagnosis is very similar to the previous case of the Noto Peninsula (Asa et al., 2007). The speed factor exceeded 10 at 14-17Z in Ryotsu Bay (Fig. 6d). These features have been simulated by the parent model (DR_M) only crudely.

The time-series of along-shore velocity components of in-situ measurement (Igeta et al., 2015) and model results show the dominance of the inertial frequency again (Fig. 7). The response of the DR_C model to the meteorological disturbances is comparable to (or even stronger than) the measured data. But the simulated amplitude of DR_M is too weak at S2, which is surrounded by land cells. Higher resolution is therefore required for the simulation of kyucho in this bay.

The clockwise intrusion of the strong kinetic energy can be partly validated by the peak time of the coastal current. We do not find a strong southward current at S1 prior to S2, but the strong northward current commonly appears several hours late compared with the southward current at S2 in the two measured events (Fig. 7). A similar lag of 4 to 8 hours is found in the DR_C model experiment. The delayed response at S1 is also visible in Fig. 6e. Thus, the propagation of stormy current is not always along the coastline.

After a few cycles of inertial motion, a small-scale eddy can be formed as shown in

Fig. 6f. This clockwise eddy may be recognized as a lee eddy of the TWC behind Sado Island. The northward current measured at S1 for the same period also supports the separation of a downstream eddy (Fig. 7b).

3.4 Wakasa Bay

The generation of topographically-constrained eddy is better known in Wakasa Bay (e.g., Wada and Yamada, 1997). The bay-scale clockwise eddy was actually captured by the downward-looking ADCP measurements with the research vessel “Fukui-maru” in September 16, 2010, as shown in Fig. 8. This measurement was carried out by a prompt cruise after set-net damage that occurred on the previous day. Kaneda et al (submitted) have suggested that the clockwise eddy was extremely strong and that its propagation probably destroyed the set-net structure near Cape Echizen at the eastern coast of Wakasa Bay.

The DR_C model also produces the clockwise eddy in the present experimental period, as shown by Fig. 9. The eddy structure closely resembles with the measured features of the eddy, such as the horizontal scale ($\sim 30\text{km}$) and central location ($\sim 35^{\circ}50'N$, $135^{\circ}45'E$), presence of the coastal current from the Tango Peninsula, and even weak eastward current along the southern coast ($\sim 35^{\circ}36'N$).

Meteorological disturbances can often be identified as the cause of the bay-scale eddy. The northward or eastward wind is enhanced due to DIANMU passage in August 11. The offshore surface water immediately starts its near-inertial oscillation as a response to the changes of wind (with the inertial period ~ 20.5 hour at $35^{\circ}50'N$). At the same time, coastal waves can be set up along the San-in Coast and be propagated to the Tango Peninsula. Abnormal kinetic energy can actually intrude to the western part of Wakasa Bay (southeast of the Tango Peninsula), as shown in Fig. 10b. In fact, the set-net fisheries around the Tango Peninsula were significantly damaged in August 12-13 (Kumaki, 2012).

According to our simulation, this kyucho was then transformed into a clockwise vortex that separated from the Tango Peninsula (Fig. 10c). The sequence from the rapid current intrusion to the lee eddy is quite similar to the previous case for Sado Island. Therefore, the interaction of the coastal current and coastal geometry is the key factor for the generation of downstream eddies. Assuming a typical speed ~ 1 m/s, peninsula scale ~ 20 km, and eddy viscosity ~ 100 m^2/s , the Reynolds number can be estimated to be 200, which is within the non-stationary eddy regime indeed.

The difference between this clockwise vortex and the Sado case is the presence of

coastline not only for the upstream side but also in the downstream direction. The separated eddy propagates and grows to the east (Fig. 10d), and then reaches to a near-stationary phase (Fig. 10e-f). The geostrophic balance has been established and the anticyclonic eddy lasts for more than a week. Since the horizontal scale of this eddy (~30km) coincides with the meridional extent of Wakasa Bay, the geographical constraint may be the limiting factor for the growth of this hazardous eddy.

Similarly, the formation of other bay-scale eddies can also be traced back to instability of the coastal current caused by the rapid changes in the surface meteorological condition. The strong wind events over 10 m/s marked by “a” through “d” in Fig. 11 possibly lead the development of the bay-scale eddy shown in Fig. 9. The lead time is 7-8 days for cases “a” and “b”, but it is only 2 days for “c” and “d”. Because the lee eddy has been generated more frequently in September, eddy-eddy interaction may prevent clear definition of the lead time.

It is noted that the downstream eddy does not always develop to the bay scale. A clockwise eddy was generated at the western part of Wakasa Bay in response to a strong wind event on September 23 and 24, but this eddy dissipated away while propagating to the east (not shown). One reason may be the absence of the coastal branch of the TWC. The coastal current was strong up until this wind event but then suddenly disappeared after September 23. Thus, the kinetic energy is no longer supplied from the mean flow for the development of the clockwise eddy.

We have conducted a sensitivity experiment to demonstrate the effects of the coastal current. All the model configurations, including the surface meteorological conditions, stay the same as the standard run from July to September of 2010, but the open boundary condition and the nudging target of temperature and salinity are switched to the DR_M conditions in summer 2009.

As a result, none of the bay-scale eddies were formed in this sensitivity experiment (not shown). The TWC was much weaker in summer 2009 than it was in summer 2010 as shown in Fig. 12. Here we confirm that the presence of the coastal current is indeed an important condition for the development of clockwise bay-scale eddies in Wakasa Bay.

4. Discussion and summary

We have presented a realistic numerical simulation of abrupt current occurrences (kyucho) based on a high-resolution version of the RIAM Ocean Model. Many features of the strong current were comparable between the present model and in-situ measurement

data at near-inertial scales (~ 20 hour). The minimum grid spacings of 1.5km and 2m in horizontal and vertical directions, respectively, allow for the detailed response of coastal waters to meteorological disturbances such as extratropical cyclones or typhoons. Typhoon 1004 (DIANMU) excited the surface water speed 3-5 times larger than the normal condition for most of the offshore area. On the other hand, the response factor of inshore water often exceeded 10, which is a hazardous level, from San-in Coast to Sado Island. Igeta et al. (2009) have already shown that surface responses, similar to those that we have simulated here, can accumulate near the coastal boundary and be enhanced by complex topography.

The initial processes of generation and propagation of the strong current were similar at the three coastal regions around the Tango Peninsula, the Noto Peninsula, and Sado Island. The near-inertial motion was excited by meteorological disturbances and was then propagated in the clockwise direction along the inertial circle, which often coincided with the meandering coastline. After the intrusion of kyucho into each bay, a clockwise vortex is frequently generated near the coastline. The vortex is usually released from the Tango Peninsula or from Sado Island to the east. However, for the case of the Noto Peninsula, this vortex seems to be trapped in Iida Bay ($\sim 37.4^\circ\text{N}$, 136.3°E in Fig. 4b), as pointed out by Nakada et al. (2014).

The vortex that separates from Sado Island dissipates in several days, according to the present simulation. However, the vortex possibly grows into an anticyclonic eddy in Wakasa Bay. In fact, the unique evolution of a clockwise eddy in Wakasa Bay has been frequently reported from measurement data since Uda (1931). We were able to numerically produce the realistic patterns of the bay-scale eddy in this study. It is found that the strong shear that is temporarily generated by meteorological disturbances between the coastal branch of the TWC and the land-sea boundary triggers the separation of a clockwise vortex at the lee side of the Tango Peninsula. The separated eddy grows into Wakasa Bay as the rich kinetic energy can be supplied from the mean flow of the TWC. Meanwhile, geostrophic adjustment is established and the anticyclonic eddy can be relatively stable at bay scale. Therefore, the generation of anticyclonic eddies may be predictable based on the key factors of coastal current and wind conditions. In fact, the four strong wind events preceded the formation of every bay-scale eddy in summer 2010. The coastal current at the bay mouth was also a necessary condition as demonstrated by a sensitivity experiment in this study.

The additional experiment with thicker mixing condition of winter showed almost no occurrence of kyucho anywhere in the model region. The surface response to meteorological disturbances may be intensified with the seasonal stratification in

summer. Thus the detailed three-dimensional density structure is preferable as the initial condition for more accurate prediction of kyuchos.

Motivated by the good agreement of this numerical model to in-situ measurement data, we have already started an operational forecast of the coastal conditions online (<http://dreams-c.riam.kyushu-u.ac.jp/>). The maximum predictability of a kyucho occurrence is expected to be one week according to the time scale of bay-scale eddy development revealed in this study. Even a lead time of only a few days will be incredibly helpful for evacuating set-net components. However, actual predictability will also depend on the accuracy of meteorological forecasts.

The operational numerical forecast of strong currents may help us to more reliably and securely predict the occurrence of kyucho events. For instance, damage was reported from several set-net operators around the Noto Peninsula following the extratropical cyclone in July 2010, but, in the following month, almost nothing was claimed despite the DIANMU invasion. The occurrence of gusty currents after typhoon passage was already known to local fishery officers and operators, but such developing extratropical cyclones might easily be missed. An objective forecast with a high-resolution dynamical model will help to predict various types of stormy currents.

Acknowledgements

The authors appreciate constructive comments on this study made by Prof. Tomoharu Senjyu, Prof. Satoshi Nakada, Prof. Yujiro Kitade, Prof. Yign Noh, Dr. Takahiro Endoh, and Mr. Toshihiro Tsuji. This study was supported by the Research Project for Utilizing Advanced Technologies in Agriculture, Forestry, and Fisheries in Japan.

References

- Asa, Y., N. Hirose, T. Senjyu, 2007. Numerical simulation of kyucho along the eastern coast of the Noto Peninsula in 2004, *Oceanography in Japan*, 16, 39–50. (in Japanese with English abstract)
- Gent, P. R., J. C. McWilliams, 1990. Isopycnal mixing in ocean circulation models. *J. Phys. Oceanogr.*, 20, 150–155.
- Gill, A. E., 1982. *Atmosphere-Ocean Dynamics*, Academic Press, 662pp.

- Griffies, S. M., and R. W. Hallberg, 2000. Biharmonic friction with a Smagorinsky-like viscosity for use in large-scale eddy-permitting ocean models, *Monthly Weather Review*, 128, 2935–2946.
- Hirose, N., C.-H. Kim, and J.-H. Yoon, 1996. Heat budget in the Japan Sea, *J. Oceanogr.*, 52, 553–574.
- Hirose, N., 2011. Inverse estimation of empirical parameters used in a regional ocean circulation model, *J. Oceanogr.*, 67, 323–336.
- Hirose, N., K. Takayama, J.-H. Moon, T. Watanabe, and Y. Nishida, 2013. Regional data assimilation system extended to the East Asian marginal seas, *Umi to Sora (Sea and Sky)*, 89, 43–51.
- Igeta, Y., Y. Kitade, and M. Matsuyama, 2007. Numerical experiment on Kyucho around the Tango Peninsula induced by Typhoon 0406. *J. Oceanogr.*, 63, 835–847.
- Igeta, Y., Y. Kumaki, Y. Kitade, T. Senjyu, H. Yamada, T. Watanabe, O. Katoh, and M. Matsuyama, 2009. Scattering of near-inertial internal waves along the Japanese coast of the Japan Sea, *J. Geophys. Res.*, 114, C10002.
- Igeta, Y., K. Yamazaki, and T. Watanabe, 2015. Amplification of coastal-trapped waves resonantly generated by wind around Sado Island, Japan. *J. Oceanogr.*, 71, 41–51.
- Ishizaki, H., and T. Motoi, 1999. Reevaluation of the Takano–Oonishi scheme for momentum advection on bottom relief in ocean models, *J. Atmos. Ocean. Tech.*, 16, 1994–2010.
- Kaneda, A., K. Ayukawa, N. Hirose, J. Tsuzuki, T. Senjyu, Y. Kumaki, Y. Igeta, and T. Watanabe, 2016. Sudden strong current generated by an eddy in the eastern part of Wakasa Bay, Japan, *J. Oceanogr.*, submitted.
- Kondo, J., 1975. Air-sea bulk transfer coefficients in diabatic conditions, *Bound.-Layer Meteor.*, 9, 91–112.
- Kumaki, Y., 2012. Studies on the Kyucho around the coast of Tango Peninsula, Special Report, 9, Kyoto Institute of Oceanic and Fishery Science, 38pp. (in Japanese with English abstract)
- Kumaki, Y., Y. Kitade, and T. Tojima, 2012. Mae-kyucho along the coast of Tango Peninsula, *Oceanography in Japan*, 21, 201–217. (in Japanese with English abstract)
- Lee, H.-C., 1996. A numerical simulation for the water masses and circulations in the Yellow Sea and the East China Sea. Ph.D. thesis, Kyushu Univ., 150 pp.
- Lee, H. J., J.-H. Yoon, H. Kawamura, and H.-W. Kang, 2003. Comparison of RIAMOM and MOM in modeling the East Sea/Japan Sea circulation, *Ocean and Polar Research*, 25, 287–302.

- Matsumoto, K., T. Takanezawa, and M. Ooe, 2000. Ocean tide models developed by assimilating TOPEX/POSEIDON altimeter data into hydrodynamical model: A global model and a regional model around Japan. *J. Oceanogr.*, 56, 567–581.
- Maruyama, K., 2009a. The situation of set-nets damage by Kyucho, *Bull. Jpn. Soc. Sci. Fish.*, 5, 881–882. (in Japanese)
- Maruyama, K., 2009b. Changes of current and water temperature in Ryotsu Bay caused by Typhoon 0613, *Bull. Niigata Pref. Fish. Mar. Res. Inst.*, 2, 45–49. (in Japanese with English abstract)
- Nakada, S., N. Hirose, T. Senjyu, K. Fukudome, T. Tsuji, and N. Okei, 2014. Operational ocean prediction experiments for smart coastal fishing, *Prog. Oceanogr.*, 121, 125–140.
- Noh, Y., and H.-J. Kim, 1999. Simulations of temperature and turbulence structure of the oceanic boundary layer with the improved near-surface process. *J. Geophys. Res.*, 104, 15621–15634.
- Okei, N., J. Okuno, T. Tsuji, and T. Senjyu, 2012. Determining the features of meteorological conditions inducing Kyucho around the Noto Peninsula, aiming to prevent the Kyucho disasters, *Bull. Jpn. Soc. Fish. Oceanogr.*, 76, 131–140. (in Japanese with English abstract)
- Smagorinsky, J., 1963. General circulation experiments with the primitive equations. 1. The basic experiment, *Mon. Weather Rev.*, 91, 99–164.
- Sweby, P. K., 1984. High resolution schemes using flux limiters for hyperbolic conservation laws, *SIAM Journal of Numerical Analysis*, 21, 995–1001.
- Uda, M., 1931. Hydrographical investigations of the Wakasa Bay and its adjacent seas, *Bull. Fish. Res. Inst.*, 2, 17–35. (in Japanese with English abstract)
- Umatani, S., and T. Yamagata, 1987. Evolution of an isolated eddy near a coast and its relevance to the “Kyucho”, *J. Oceanogr. Soc. Japan*, 43, 197–203.
- Wada, Y., and H. Yamada, 1997. Flow patterns in Wakasa Bay, Japan Sea, *Bull. Japan Sea Natl. Fish. Res. Inst.*, 47, 1–12. (in Japanese with English abstract)
- Webb, D. J., B. A. de Cuevas, and C. S. Richmond, 1998. Improved advection schemes for ocean models, *J. Atmos. Oceanic Tech.*, 15, 1171–1187.

Figure captions

Fig. 1. Bottom topography of the parent (DR_M) and child (DR_C) models. Thick contours show 100 and 1000 m depths. (b) Thin contours indicate 20, 50, 200, 500, 2000, and 5000 m depths. The capital letters “TG”, “WB”, “EK”, “NT”, “TB”, “SD”, and “RB” indicate Tango Peninsula, Wakasa Bay, Echizen-Kaga Coast, Noto Peninsula, Toyama Bay, Sado Island, and Ryotsu Bay, respectively.

Fig. 2. Simulated velocity distribution by the DR_C model at 10m depth under the passage of Typhoon 1004 (DIANMU). The vectors are plotted at 5 grid interval (~ 7.4 km). The magnitude is given by the color scale shown in each diagram. Any motion weaker than 10 cm/s is omitted.

Fig. 3. (a) Maximum water speed at 10m depth during the three days from 00Z, 8/11, 2010 with a contour interval of 50 cm/s. (b-f) Same as (a) but divided by the scalar average over three months from July to September, 2010. The contour interval is 2.

Fig. 4. Horizontal velocity field at 10 m depth at the time of a kyucho arrival to Stn.N2 (06-07Z, 7/12, 2010) in Toyama Bay modeled by (a) DR_M, (b) DR_I, and (c) DR_C. The open and thick vectors show speeds larger than 50 and 100 cm/s, respectively. Weak motions smaller than 10 cm/s are omitted.

Fig. 5. Time series of alongshore velocity component in cm/s for one week from 00Z of (a,c) July 10 or (b,d) August 10 at 10m depth at (a,b) N1 of $37^{\circ}26'N$, $137^{\circ}22'E$ and (c,d) N2 of $37^{\circ}17'N$, $137^{\circ}11'E$, whose locations are indicated in the previous figure. The gray and black curves show the parent and child model (DR_M and DR_C) results, respectively. The dots are given by in-situ measurement.

Fig. 6. Sequence of surface velocity changes associated with Typhoon 1004 (DIANMU). The five diagrams (a-e) are given by one-hour averages but the last one (f) is 39 hour (~ 2 inertial cycles) mean. Weak motions smaller than 10 cm/s are omitted. Gray and black grids show normalized speeds larger than 4 and 8, respectively.

Fig. 7. Same as Fig. 5 but at (a,b) S1 of $38^{\circ}19'N$, $138^{\circ}32'E$ and (c,d) S2 of $38^{\circ}08'N$, $138^{\circ}27'E$.

Fig. 8. Horizontal velocity measured by ADCP of R/V Fukui-maru on September 16, 2010. The vector scale is shown at the northwestern part.

Fig. 9. Horizontal velocity field at each maximum growth of the warm eddy at 10m depth in Wakasa Bay. These velocity components are based on 21-hour (~inertial period) averages from 1:00Z to 22:00Z at (a) 8/5, (b) 8/17, (c) 9/10, and (d) 9/15 of 2010. The speeds smaller than 10 cm/s are eliminated.

Fig. 10. Typical evolution of the clockwise eddy pinched off from the TWC near the Tango Peninsula into Wakasa Bay. The vectors are plotted every three grid for the longitudinal direction.

Fig. 11. Time series of surface wind speed in m/s derived from the GPV/MSM model north of the Tango Peninsula (35.8-36.0°N, 135.0-135.25°E).

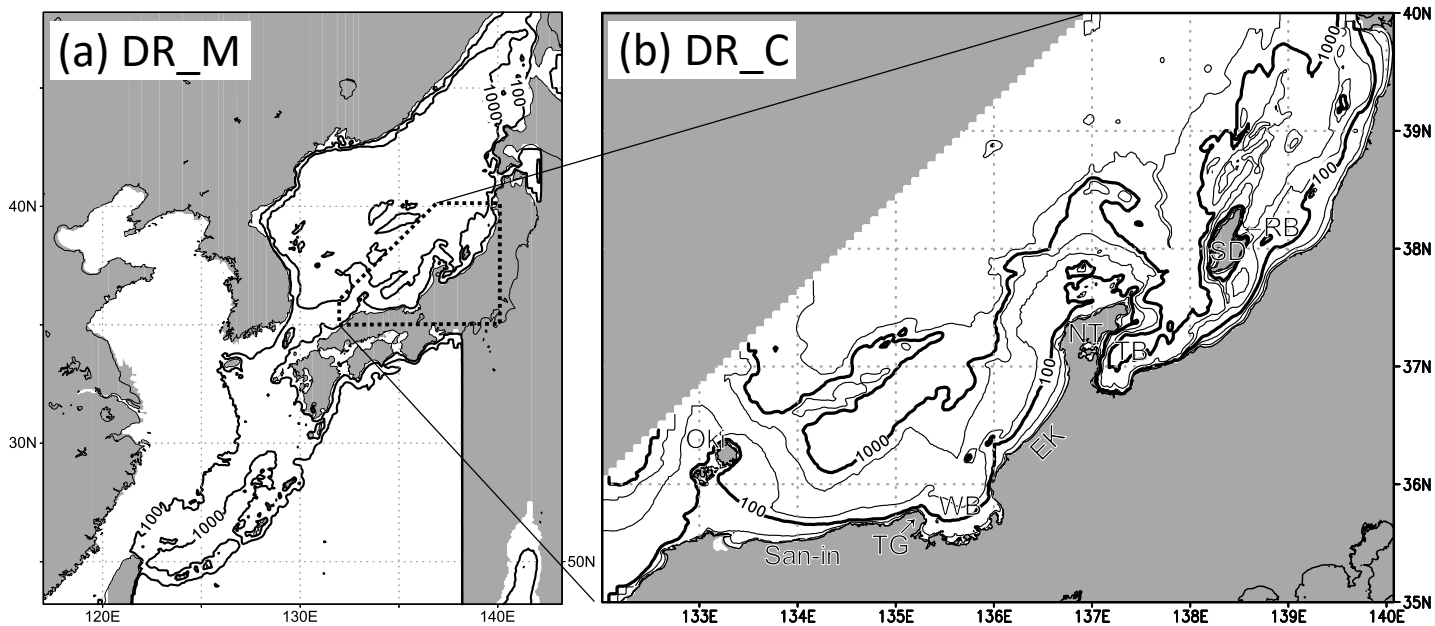
Fig. 12. Monthly-mean horizontal velocity for August of (a) 2009 and (b) 2010 based on the data assimilation model of DR_M. The speeds smaller than 5 cm/s are eliminated.

Tables

Table 1. Major differences in the configurations of the three models compared in this study.

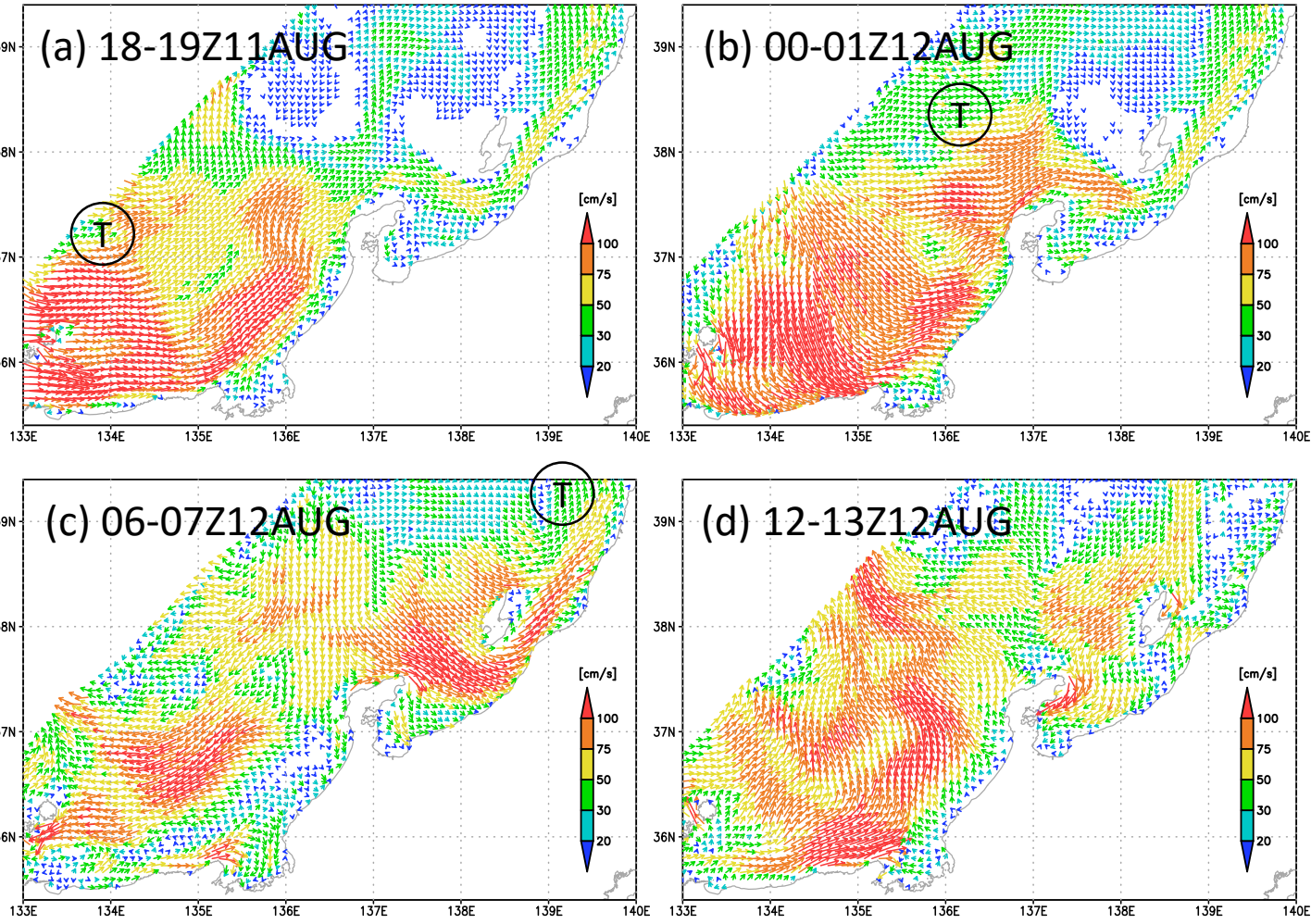
	DR_M	DR_I	DR_C
domain	Japan and East China Seas	around Noto Pen.	from San-in Coast to Sado Is.
$\Delta x \times \Delta y$	5' \times 4' (~7.4km)	1' \times 0.8' (~1.5km)	←
top Δz	8 m	←	2 m
grid number	320 \times 384 \times 38	192 \times 256 \times 34	485 \times 384 \times 36
barotropic and baroclinic Δt	6 and 120 sec	2 and 20 sec	←
horizontal eddy viscosity	biharmonic + harmonic	←	Smagorinsky (1963)
surface forcing	JMA-GSM, 6-hourly	JMA-MSM, hourly	←
open boundary condition	DR_B (Hirose, 2011) + tide (Matsumoto et al., 2000)	DR_M	←
data assimilation	Yes	No	←
publication	Hirose et al. (2013)	Nakada et al. (2014)	This study

Fig. 1



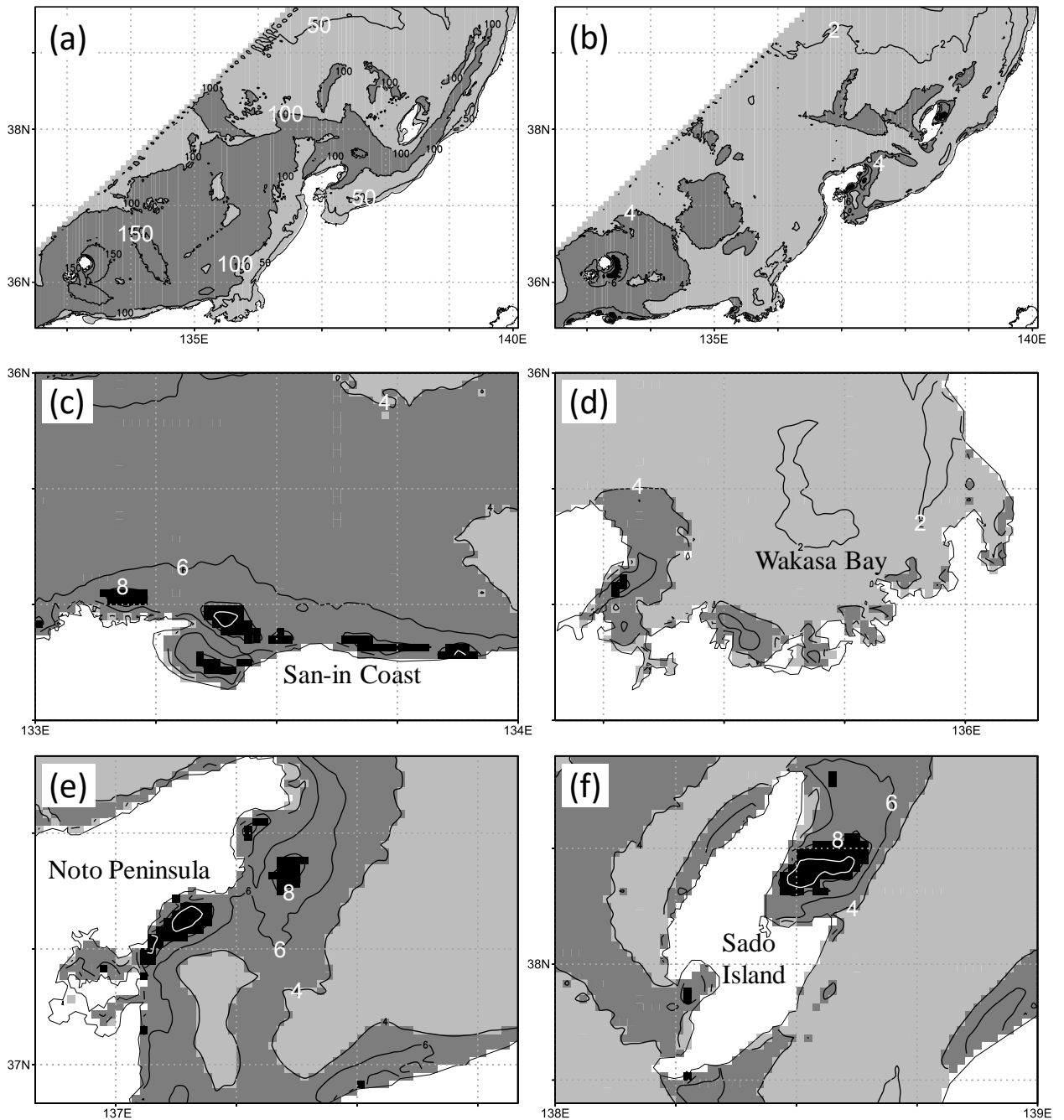
Bottom topography of the parent (DR_M) and child (DR_C) models. Thick contours show 100 and 1000m depths. (b) Thin contours indicate 20, 50, 200, 500, 2000, and 5000m depths. The capital letters “TG”, “WB”, “EK”, “NT”, “TB”, “SD”, and “RB” indicate Tango Peninsula, Wakasa Bay, Echizen-Kaga Coast, Noto Peninsula, Toyama Bay, Sado Island, and Ryotsu Bay, respectively.

Fig. 2



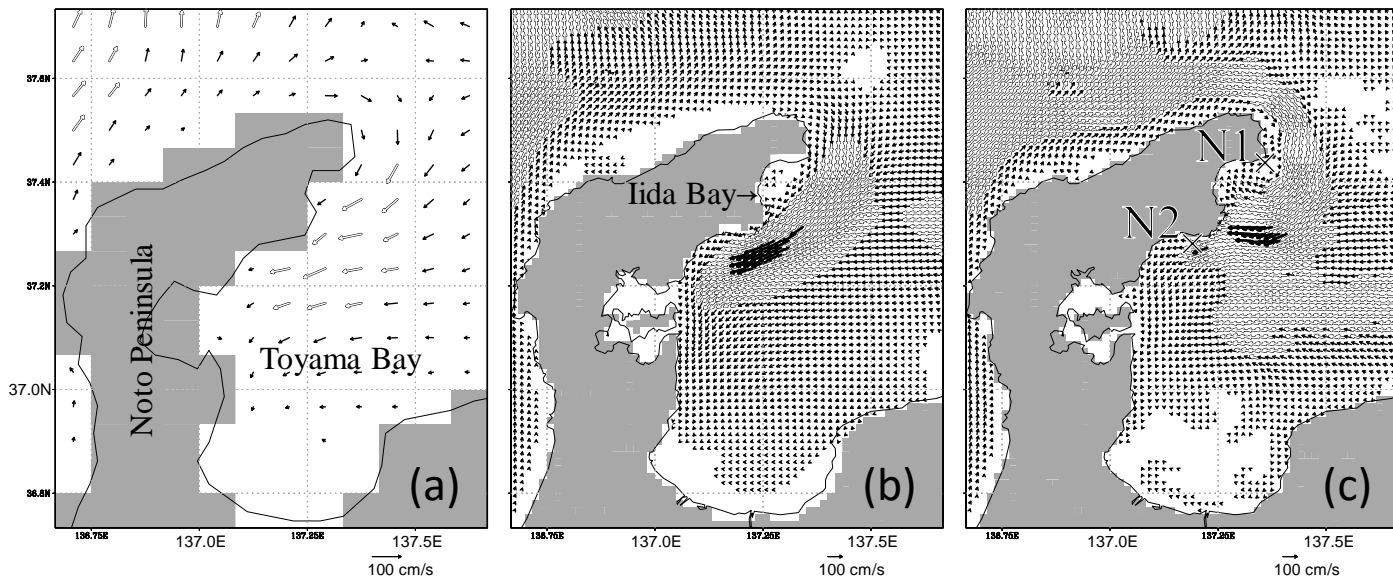
Simulated velocity distribution by the DR_C model at 10m depth under the passage of Typhoon 1004 (DIANMU). The vectors are plotted at 5 grid interval (~7.4km). The magnitude is given by the color scale shown in each diagram. Any motion weaker than 10cm/s is omitted.

Fig. 3



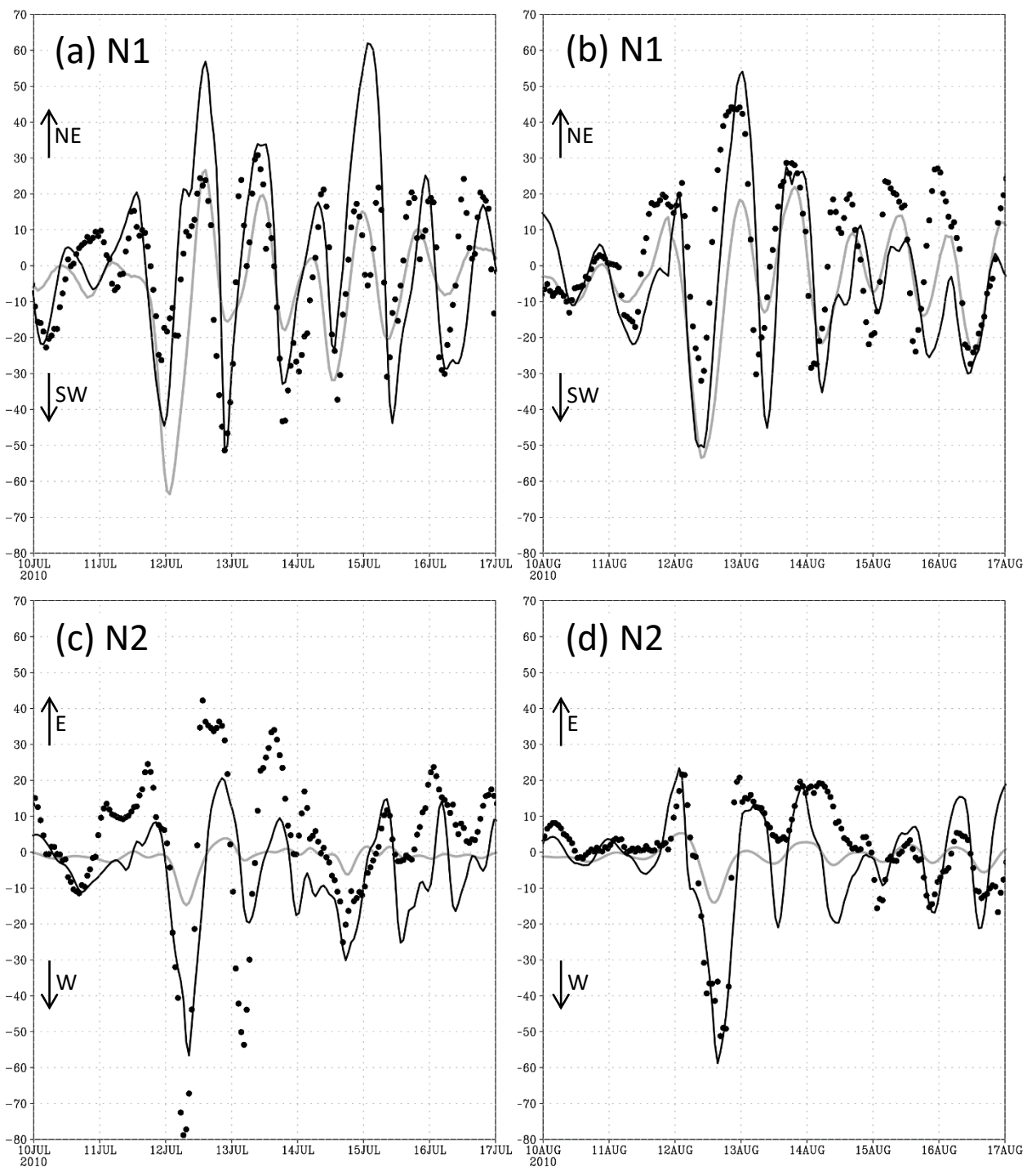
(a) Maximum water speed at 10m depth during the three days from 00Z 8/11, 2010 with a contour interval of 50cm/s. (b-f) Same as (a) but divided by the scalar average over three month from July to September, 2010. The contour interval is 2.

Fig. 4



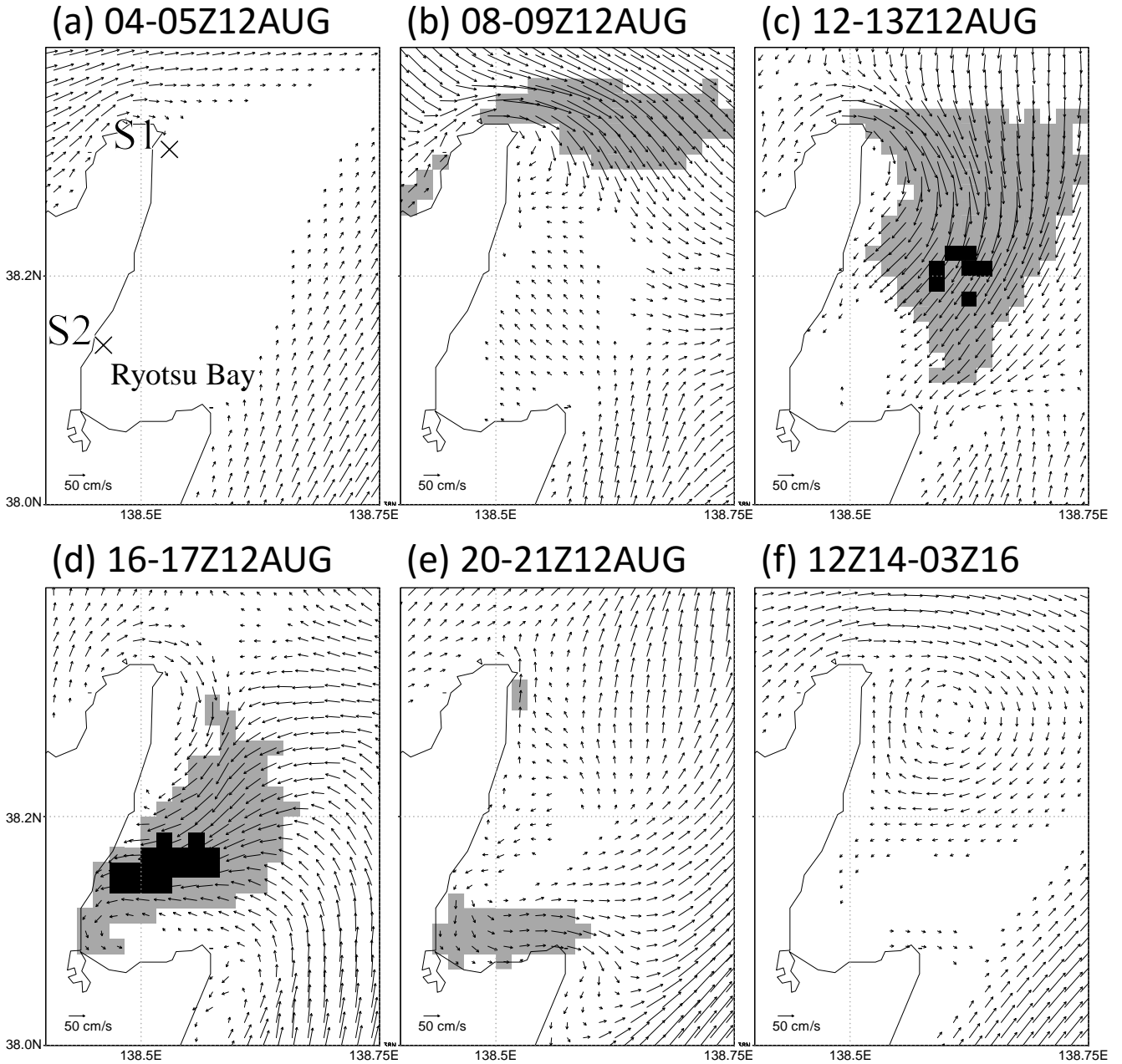
Horizontal velocity field at 10 m depth at the time of a kyucho arrival to Stn.N2 (06-07Z of 7/12, 2010) in Toyama Bay modeled by (a) DR_M, (b) DR_I, and (c) DR_C. The open and thick vectors show the speed larger than 50 and 100cm/s, respectively. Weak motions smaller than 10cm/s are omitted.

Fig. 5



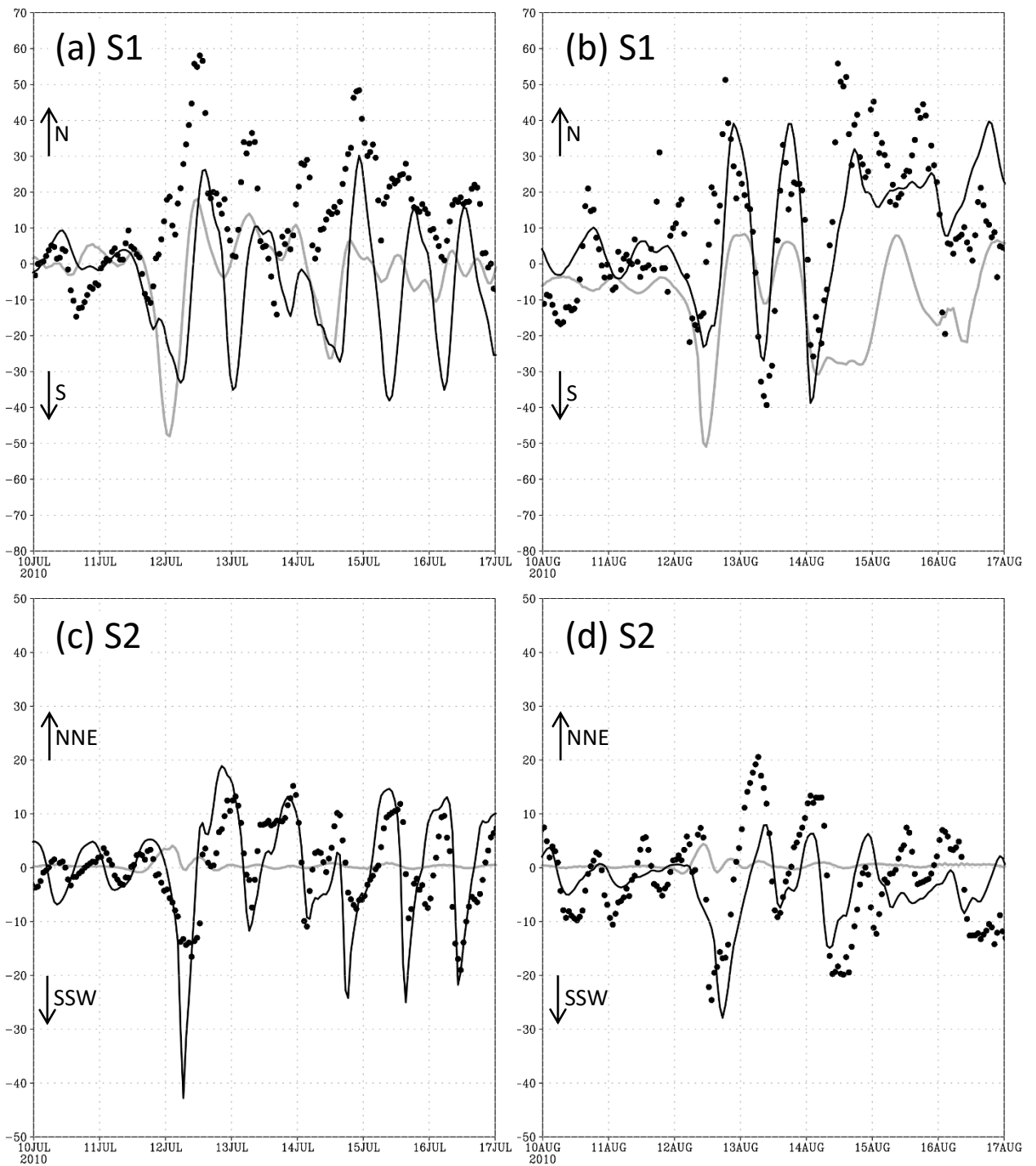
Time series of alongshore velocity component in cm/s for one week from 00Z of (a,c) July 10 or (b,d) August 10 at 10m depth at (a,b) N1 of $37^{\circ}26'N$, $137^{\circ}22'E$ and (c,d) N2 of $37^{\circ}17'N$, $137^{\circ}11'E$, whose locations are indicated in the previous figure. The gray and black curves show the parent and child model (DR_M and DR_C) results, respectively. The dots are given by in-situ measurement.

Fig. 6



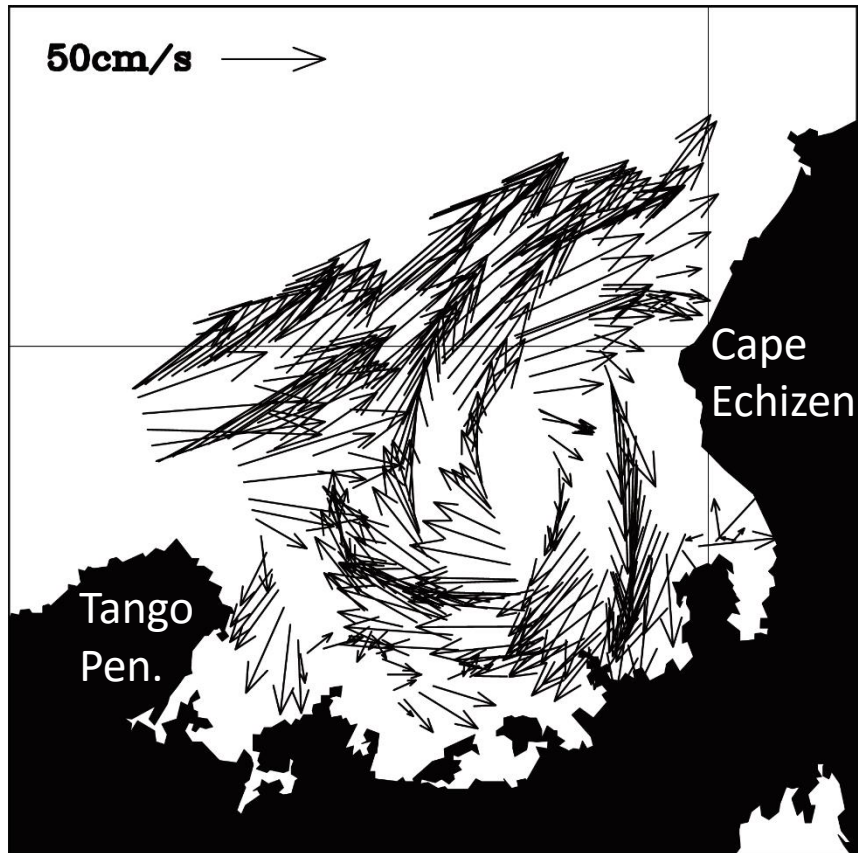
Sequence of surface velocity change associated with Typhoon 1004 (DIANMU). The five diagrams (a-e) are given by one-hour averages but the last one (f) is 39 hour (~ 2 inertial cycles) mean. Weak motions smaller than 10cm/s are omitted. Gray and black grids show normalized speeds larger than 4 and 8, respectively.

Fig. 7



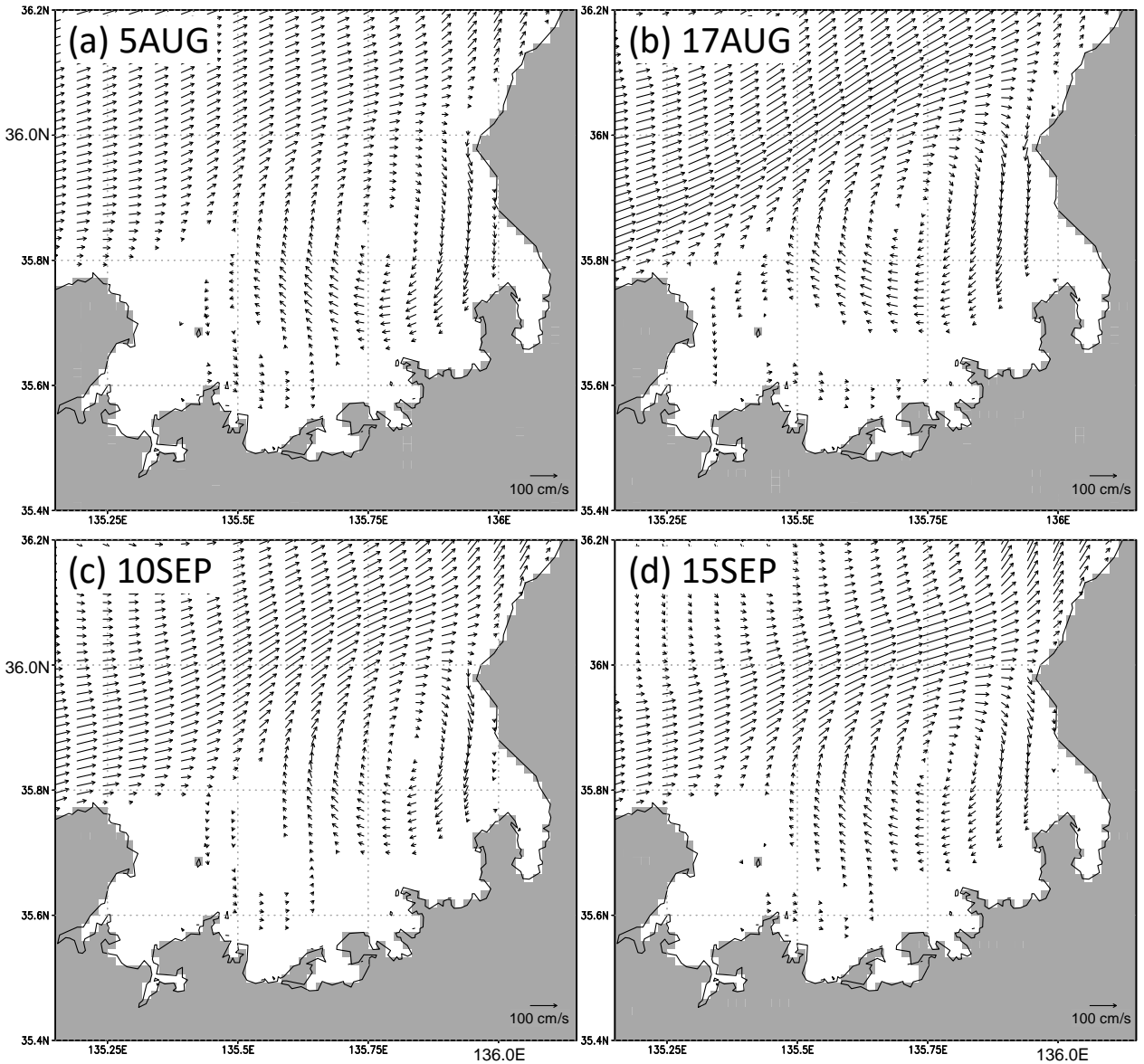
Same as Fig. 5 but at (a,b) S1 of $38^{\circ}19'N$, $138^{\circ}32'E$ and (c,d) S2 of $38^{\circ}08'N$, $138^{\circ}27.5'E$.

Fig. 8



Horizontal velocity measured by ADCP of R/V Fukui-maru on September 16, 2010. The vector scale is shown at the northwestern part.

Fig. 9



Horizontal velocity field at each maximum growth of the warm eddy at 10m depth in Wakasa Bay. These velocity components are based on 21-hour (~inertial period) averages from 1:00Z to 22:00Z at (a) 8/5, (b) 8/17, (c) 9/10, and (d) 9/15 of 2010. The speeds smaller than 10cm/s are eliminated.

Fig. 10

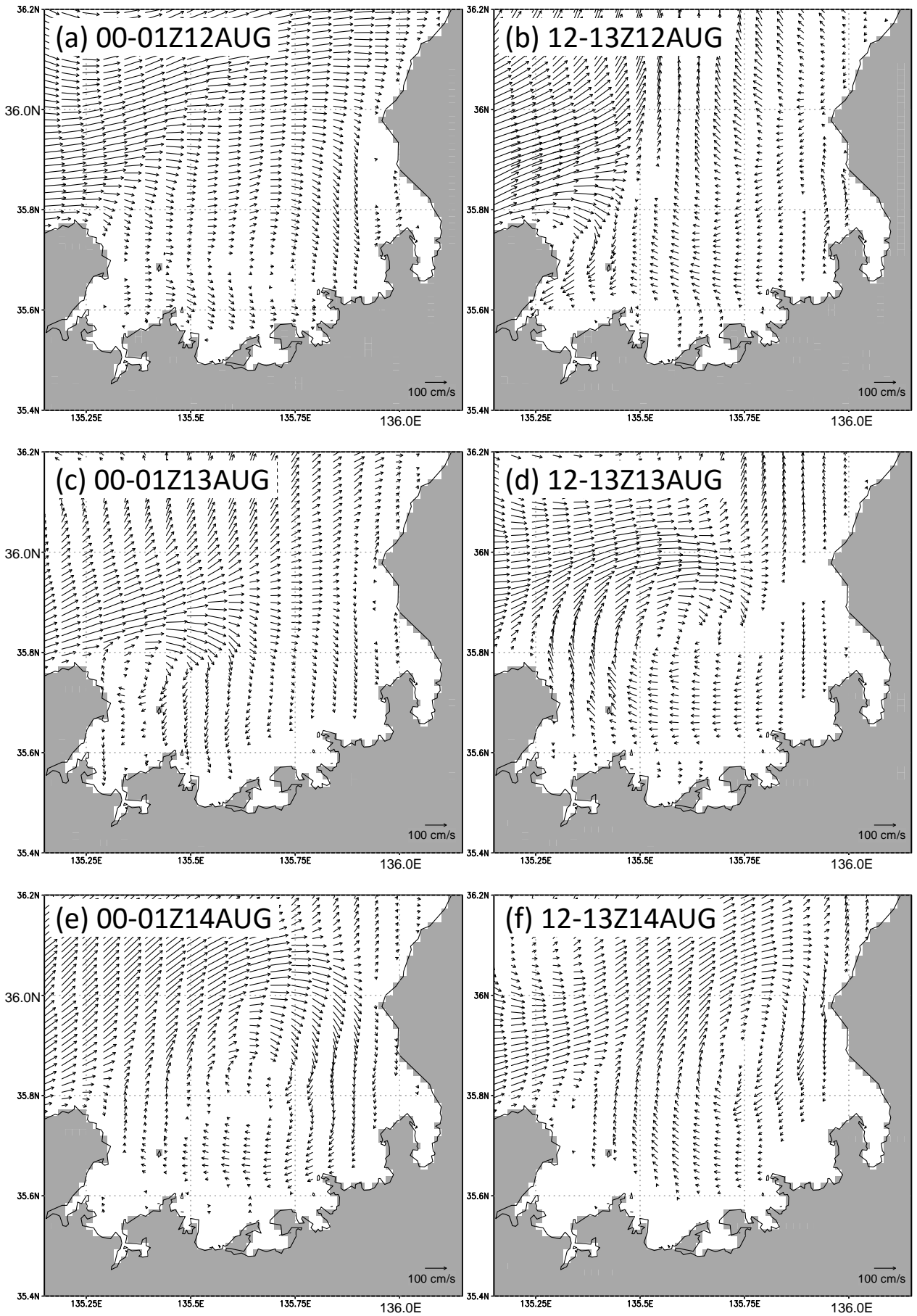
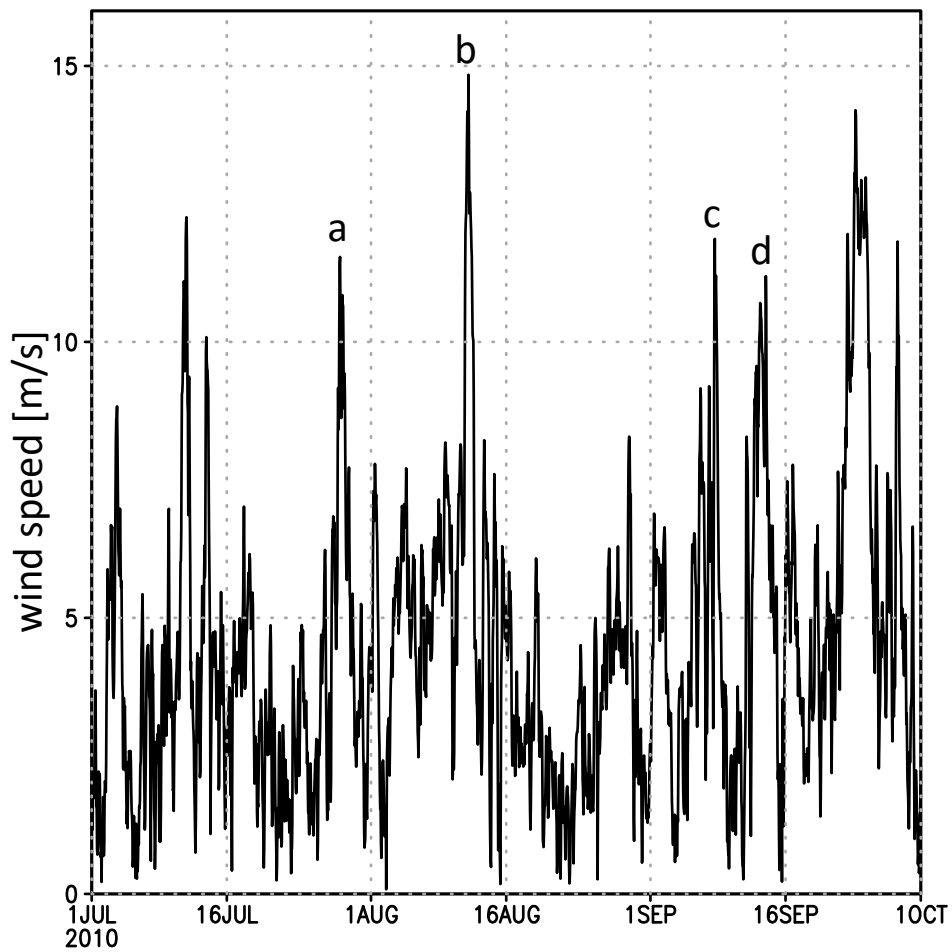
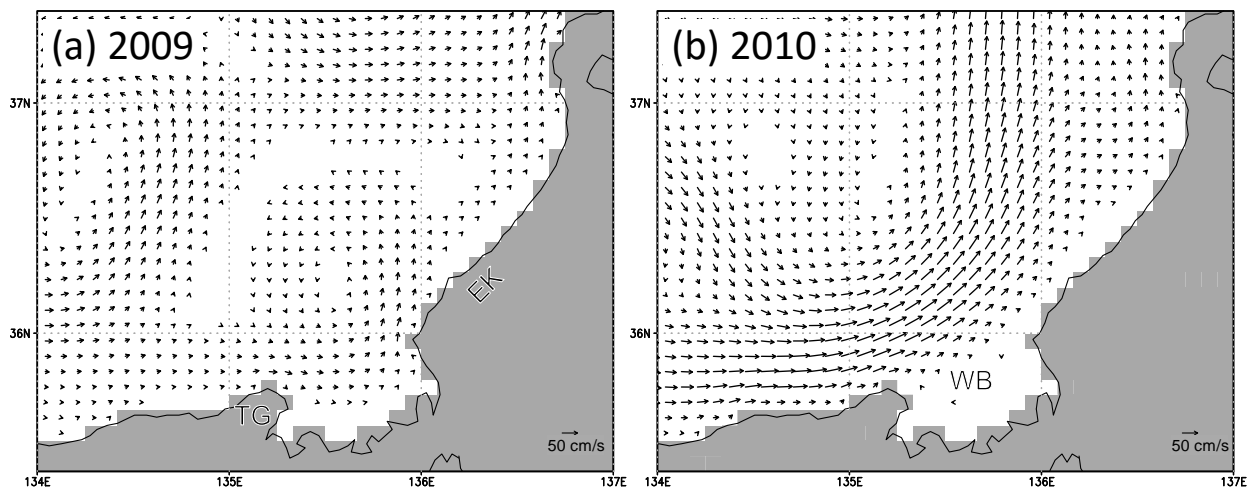


Fig. 11



Time series of surface wind speed in m/s derived from the GPV/MSM model north of the Tango Peninsula ($35.8-36.0^{\circ}\text{N}$, $135.0-135.25^{\circ}\text{E}$).

Fig. 12



Monthly-mean horizontal velocity for August of (a) 2009 and (b) 2010 based on the data assimilation model of DR_M. The speeds smaller than 5cm/s are eliminated.